
MRI and MR Arthrography

Emma L. Rowbotham and Andrew J. Grainger

Contents

1	Introduction	38
2	Technical Considerations	38
2.1	Positioning	38
2.2	Imaging Planes	39
2.3	Sequences.....	41
2.4	Artefacts.....	42
3	Imaging Findings	43
3.1	Osseous Structures.....	43
3.2	Tendons.....	44
3.3	Triangular Fibrocartilage Complex.....	45
3.4	Ligaments.....	47
3.5	Hyaline Cartilage.....	49
4	MR Arthrography	49
4.1	Protocols	50
4.2	Injection of Contrast.....	50
4.3	Artefacts.....	51
4.4	Indirect Arthrography.....	51
4.5	Alternative Modalities.....	51
5	7T Imaging	51
	References	51

Abstract

The complex anatomical nature of the hand and wrist brings about diagnostic challenges both for the Clinician and the Radiologist when considering pathology in this region. MR is a proven, widely employed imaging modality used in the detection, assessment and follow-up of disorders of both the hand and the wrist. Optimisation of both sequences and protocols are essential in order to provide good quality images which allow high sensitivity and specificity for detection of pathology. High field strength units are usually used in hand and wrist imaging alongside dedicated extremity coils. Even then, there are numerous artefacts which may be encountered including movement, pulsation, truncation, magic angle and chemical shift. These phenomena will be discussed in this chapter in addition to a brief outline of sequences and their potential uses. Pathology relating to osseous structures, tendons, TFCC and both intrinsic and extrinsic ligaments are all readily assessed on MR imaging and the optimal planes for imaging are discussed alongside common pathologies and potential pitfalls in image interpretation. MR arthrography is also discussed with particular reference to both TFCC and intrinsic ligament pathology. Recent advances in technology, including the advent of 7T units, have led to improvements in the assessment of articular cartilage at the wrist and techniques of biological imaging, which continue to evolve.

E. L. Rowbotham (✉)
Royal United Hospital, Bath, UK
e-mail: emmarowbotham@doctors.org.uk

A. J. Grainger
Department of Musculoskeletal Radiology,
Chapel Allerton Orthopaedic Centre,
Leeds, LS7 4SA, UK
e-mail: andrew.grainger@leedsth.nhs.uk

1 Introduction

The complex anatomical nature of the hand and wrist brings about diagnostic challenges both for the Clinician and the Radiologist when considering pathology in this region. However, advances in imaging techniques have allowed increasingly accurate diagnostic performance and MR imaging is a proven, widely employed imaging modality for the detection, assessment and follow-up of disorders of the hand and wrist. The radiologist requires a detailed knowledge of the anatomy and range of pathological conditions affecting the hand and wrist. However, a knowledge of the clinical information and careful consideration of the available and most appropriate imaging modalities are essential in determining the relevant technique and sequence protocols.

There are many potential pitfalls when imaging the hand and wrist, an incorrect sequence or misinterpretation of an anatomical variant may lead to inaccurate diagnosis particularly of both TFCC and intrinsic ligament pathology. This chapter will provide a review of technical considerations and MR protocols followed by discussion of the most common and most relevant clinical applications.

2 Technical Considerations

In general terms, the higher the magnetic field strength used in MR imaging the greater both the signal-to-noise ratio (SNR) and the contrast-to-noise ratio (CNR) achieved. An increased SNR allows thinner slice thickness which in turn allows greater spatial resolution and also shorter acquisition times, thereby reducing the likelihood of patient movement. Thin and contiguous slices are needed in order to accurately image the intrinsic structures of the wrist many of which are no greater than a few millimetres thick.

A high field strength magnet (1.0T or higher) is usually preferred for optimal imaging of the fine architecture of the hand and wrist; in addition a local or surface coil is necessary to ensure sufficient signal-to-noise ratio. However, for applications which rely on contrast resolution as opposed to spatial resolution—for example evaluation of radiographically occult fractures or osteonecrosis of the carpus—lower field strength extremity units (0.1–0.6T) in either

open or extremity units may suffice to answer a specific clinical question. However, in this situation cartilage lesions and subtle pathology of the tendons, ligaments and fibrocartilage will not be as readily identified. These low field strength scanners may be useful where there is limited space available within a department and for patients who are either claustrophobic or obese.

The majority of studies comparing the sensitivity and specificity of low field strength versus high field strength units in the upper limb have focussed on shoulder imaging, often with conflicting outcomes. Currently, most centres performing regular hand and wrist imaging will use at least a 1.5T unit and increasingly 3T units are becoming the norm. Thinner slices are possible with 3T imaging and CNR may be increased by a magnitude of 2.0–2.9 times that of 1.5T if all other parameters are kept constant (Saupe et al. 2005). Studies have shown the higher SNR and CNR obtained with 3T units allow significantly improved visualisation of the small anatomical structures of the hand and wrist including the scapholunate and lunotriquetral ligaments (Saupe et al. 2005). Although direct comparisons have not been undertaken, findings suggest that 3T imaging may have improved sensitivity and specificity compared to 1.5T imaging for detection of both TFCC tears and scapholunate tears (Magee 2009). Improved visualisation of the median and ulnar nerves at high field strengths imaging has also been documented (Farooki et al. 2002).

Coil selection is also vitally important in hand and wrist imaging and receiver coils with high signal-to-noise ratio capability and uniformity are needed. Surface array coils are used to provide high SNR and an extended field-of-view (Roemer et al. 1990). Studies have also shown that phased array coils and adapted birdcage head coils may be used to provide both high SNR and image uniformity (Kocharian et al. 2002). Coils continue to improve with greater numbers of elements, but the optimising coils for hand and wrist imaging remains an engineering challenge.

2.1 Positioning

In high field strength systems, there are two main options for patient positioning; the patient may lie prone within the scanner, with their symptomatic arm stretched out above the head and the wrist positioned



Fig. 1 Sagittal T2W FS image with the wrist in ulnar deviation. The lunate shows slight dorsal tilt but the long axis of the capitate remains aligned with the long axis of the radius—indicating that this appearance is due to physiological positioning

within the isocentre of the magnet, thereby allowing for homogenous fat suppression, or alternatively they may lie supine with the hand and wrist at the side of the body. The latter position may prove to be more comfortable for the patient but can lead to inhomogeneous fat suppression given the wrist and hand are not central within the magnet. Motion artefact can be a significant problem and it may be more important to optimise patient comfort and accept suboptimal positioning. Motion artefact is minimised by using restraints such as foam cushions and wedges. In order that positioning abnormalities are not incorrectly diagnosed as carpal instability syndromes it is important to eliminate significant radial or ulnar deviation at the wrist. However, even correctly positioned wrists may occasionally simulate a dorsal intercalated segment instability and correlation with both clinical findings and a lateral radiograph may be helpful in this situation. It is also useful to note that the long axis of the capitate will remain centred on the long axis of the radius when the lunate undergoes physiological extension, while in a

true DISI deformity there will be dorsal translation of the long axis of the capitate (Fig. 1).

The degree of pronation and supination of the wrist will influence the appearances of the distal radioulnar joint (DRUJ). Ideally, MRI is obtained with the wrist in a neutral position as pronation and supination can mimic dorsal and volar subluxation of the ulnar at the DRUJ. It is important to consider wrist positioning before diagnosis of DRUJ subluxation is made (Fig. 2a, b). Pronation and supination also influence the appearance of the relative length of the radius and ulnar. The ulnar appears longer relative to the radius in pronation.

For imaging of the fingers, both supine (with the arm at the side of the body) and prone (with the arm above the head) positions are described in the literature and are accepted techniques for producing good image quality (Blackband et al. 1994). As with wrist imaging positioning within the centre of the magnetic field is vitally important in imaging the fingers. Generally, the fingers are imaged when fully extended, however the flexed position (around 45 degrees), may be of value in evaluating possible pulley lesions as well as collateral ligament injury (Hauger et al. 2000).

For imaging individual finger joints a surface microscopy coil may be useful (Tan et al. 2005). If both hands or both wrists are to be imaged on the same patient then a larger extremity coil may be used to image both sides at one time thereby decreasing the scan time required. The hands and wrists can be placed palm together with the arms above the head both within the coil.

2.2 Imaging Planes

Typically protocols for the hand and wrist include images acquired in all three orthogonal planes. Imaging the thumb presents particular difficulties for alignment of planes as it does not lie in an orthogonal plain relative to the hand and wrist. In this situation, sagittal and coronal imaging is aligned relative to the thumb metacarpal from an axial image.

2.2.1 Axial

Axial imaging is usually performed first as these sequences are then used to set up the coronal and sagittal sequences. The plane should be determined as

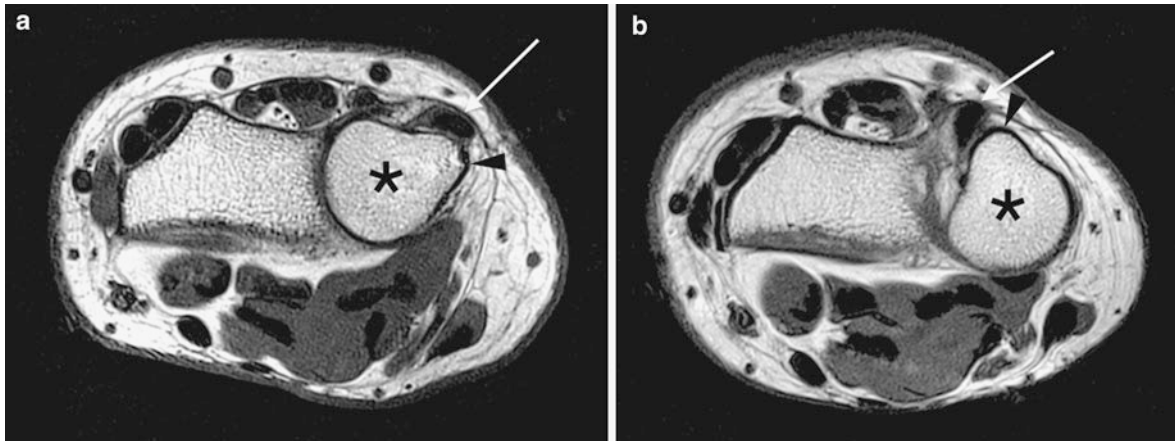


Fig. 2 **a** and **b**—Axial imaging in the same asymptomatic patient with the wrist in **a** pronation and **b** supination. With the wrist in supination appearances suggest volar subluxation of the ulnar (*asterix*) and in pronation there is dorsal subluxation of

the ulnar (*asterix*). There is also a marked change in position of the Extensor carpi ulnaris tendon (*white arrow*) between these two wrist positions. To eliminate these apparently abnormal findings it is important to image the wrist in a neutral position

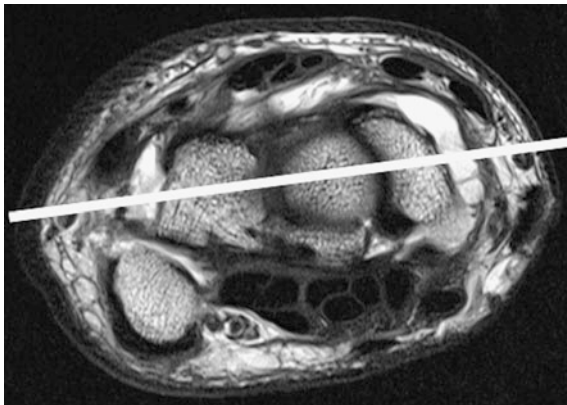


Fig. 3 The coronal plane is determined by a line bisecting the scaphoid, lunate and capitate (*yellow line*) on an axial image through the proximal carpal row

being parallel to the distal radius. For imaging of the wrist coverage should include the region between the distal radius/ulnar metaphysis proximally, extending to the proximal metacarpal shafts distally.

2.2.2 Coronal

The correct plane is crucial for coronal imaging and should be derived from an axial image through the proximal carpal row. The plane of section should bisect the scaphoid, lunate and capitate (Fig. 3). The TFCC is best demonstrated on coronal sequences, and this plane may also be used to assess both the

Fig. 4 Sagittal T2 FS image of the index finger shows both the flexor and extensor tendons as low signal structures inserting into the distal phalanx. This plane may be used to assess continuity of the tendons as well as alignment within the digit. The tendon is concave towards the proximal and middle phalanges (*black arrow*) as a result of the action of the associated pulleys at these levels. The volar plate is also demonstrated in this plane (*white arrows*)



intrinsic and extrinsic ligaments of the wrist. For imaging of the fingers the coronal plane will be determined as being parallel to the anterior volar cortex of the metacarpal heads.

2.2.3 Sagittal

The sagittal plane should be perpendicular to the coronal plane and for wrist imaging should include all soft tissues to either side of the radius and ulnar. Sagittal images are useful in determining carpal alignment and carpal instability and in the fingers the flexor and extensor tendons are best evaluated in this plane (Fig. 4).

2.3 Sequences

The exact protocols for imaging the hand and wrist will vary between institutions depending on radiologist and clinician preferences and on the scanning unit involved.

2.3.1 T1 Weighted Imaging

T1 weighted imaging is ideal for detecting marrow infiltration and is also helpful in distinguishing areas of red marrow reconversion from pathological area of change and should be included in a routine wrist protocol in at least one plane without fat saturation.

2.3.2 Fast Spin Echo

Fast Spin Echo (FSE) sequences also referred to as Turbo Spin Echo (TSE) were originally introduced in order to speed up image acquisition through the simultaneous acquisition of multiple echoes. The advantage over spin echo sequences (SE) is the reduction in acquisition time, for long TR sequences. This reduces examination time but also helps to minimise movement artefact whilst maintaining the same SNR. FSE imaging forms the basis of proton density and T2 weighted imaging widely used in clinical hand and wrist MRI. Frequency selective fat suppression will be often applied to these sequences. In addition to improving their sensitivity to water, particularly in fatty bone marrow, fat suppression will also improve contrast between bone and articular cartilage. Fat suppressed proton density FSE imaging is particularly good for imaging articular cartilage. Recently, 3D fast SE became available from some manufacturers giving the potential for thin slice contiguous images and multiplanar reconstructions. Their use is still being evaluated and evidence would suggest they are not yet suitable to replace 2D FSE imaging (Stevens et al. 2011).

2.3.3 Short T1 Inversion Recovery

Short T1 Inversion Recovery (STIR) sequences provide an alternative means to achieve fat suppression. Where a relatively short inversion time is used to null the fat signal whilst maintaining water and soft tissue signal. This technique is particularly helpful where field inhomogeneities prevent uniform fat suppression. This can be a particular problem

with hand and wrist imaging if it is not possible to position the area of interest in the isocentre of the magnet. STIR sequences are particularly useful in the detection of bone marrow abnormalities in the hand and wrist such as occult fractures. In addition the TFCC and intrinsic ligaments are often well visualised on STIR sequences. STIR images show high contrast but suffer from a low signal to noise ratio. STIR is not specific to fat and tissues with a similar T1 signal to fat will also be suppressed—this includes structures which have shown enhancement following gadolinium administration.

2.3.4 Gradient Echo

Gradient Echo images provide a high degree of spatial resolution but at the expense of relatively poor contrast resolution. In addition, 3D T1 weighted gradient echo images may be used to allow thin slice multiplanar reconstructions. These sequences show increased susceptibility artefact and therefore are of little use in the presence of metalwork, such as following surgery.

2.3.5 Typical Protocols

As already stated protocols will vary depending on preference, indication of the examination and MRI equipment. Typically, a routine wrist MRI protocol will include axial coronal and sagittal imaging using a combination of FSE proton density and T2 imaging. Fat suppressed imaging is helpful for demonstrating cartilage and improving sensitivity to fluid in bone and will usually be applied in at least two planes. It is important to include at least one non-fat suppressed T1 weighted sequence. The authors also make frequent use of thin slice 3D gradient echo sequences (GE), particularly for the evaluation of subtle bony erosions in the wrist and hand joints.

In some situations a far more limited protocol can be utilised. For instance to identify radiographically occult bone injury, particularly possible scaphoid fracture, T1 and T2 imaging in the coronal and sagittal plane may suffice.

The use of iodinated contrast may be required in some situations such as the evaluation of scaphoid non-union/avascular necrosis or for identifying synovitis (and distinguishing it from effusion) in arthritis imaging.

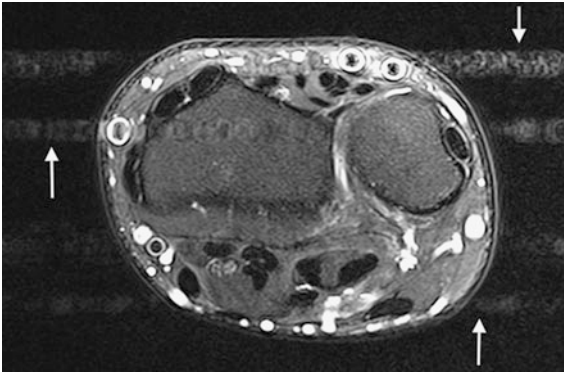


Fig. 5 T2 FSE axial image which shows several areas of flow artefact which manifests as ghosting of the vessels perpendicular to the blood flow in the direction of the phase-encoding gradient (*white arrows*)

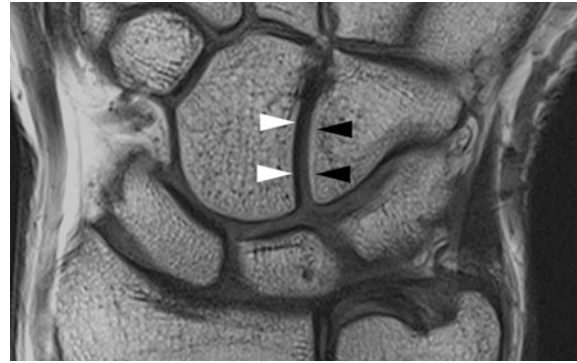


Fig. 6 Chemical shift artefact—Coronal image of the wrist which shows chemical shift artefact between the capitate and hamate. This occurs in the direction of the frequency encoding gradient and manifests as a low signal intensity band adjacent to the subchondral plate of the capitate (appearing as a thickened subchondral plate) (*white arrowheads*) and a corresponding high intensity band along the subchondral bone of the opposing articular surface of the hamate (*black arrowheads*). The effect is to give an apparent asymmetry to the thickness of the articular cartilage on the two surfaces

2.4 Artefacts

2.4.1 Motion Artefact

Motion artefact will manifest as blurring or ghosting of the images. In the hand and wrist patient movement is a common cause however pulsation artefact from vessels may also occur.

2.4.2 Pulsation Artefact

Pulsation artefact results from blood flow and can be minimised by saturation bands perpendicular to blood vessels. The effect can also be minimised by planning the phase encoding direction to cast the artefact away from anatomical structures that need to be evaluated (Fig. 5).

2.4.3 Chemical Shift Phenomena

Chemical shift phenomena are usually apparent at water–fat interfaces due to a difference in resonance frequency between fat and water; fat resonates at a slightly lower frequency than water (Larmor frequency). Both SE and GE may demonstrate chemical shift artefact which appears as a hypointense band, one to several pixels in width, towards the lower part of the gradient field, and as a hyperintense band towards the higher part of the readout gradient field. This phenomenon is more pronounced at higher field strengths and lower gradient strength. In MR imaging of the wrist, chemical shift artefact is most frequently appreciated at the cartilage–bone marrow interface (Fig. 6), and may lead to over-estimation or underestimation of the cartilage thickness.

2.4.4 Susceptibility Artefact

Susceptibility artefact is related to the internal magnetisation induced in tissues by the external magnetic field and refers to the focal loss of signal intensity and distortion of the magnetic field secondary to low proton structures such as air or metal. This form of artefact is encountered frequently in musculoskeletal imaging due to the presence of surgical hardware or clips (Fig. 7). The metallic objects produce T2 and T2* shortening which results in signal loss and geometrical distortion. This effect increases exponentially with high field strength and is one of the disadvantages when imaging at 3T and higher. Approaches to reducing susceptibility artefact include: increasing the band width and/or decreasing the TE, parallel imaging, decreasing the voxel size, or lengthening the echo train length.

2.4.5 Truncation Artefacts

Truncation artefacts may occur at interfaces between high and low signal intensity structures and appear as rings at boundaries such as bone–tissue interfaces. This artefact is related to the finite number of steps used by the Fourier transform to reconstruct an image and is reduced by utilising more frequency encoding steps.



Fig. 7 Susceptibility artefact—Coronal image of the wrist joint in a patient who had previously undergone scapholunate ligament repair. A low signal area is seen in the region of the repair secondary to susceptibility artefact arising from a metallic anchor

2.4.6 Magic Angle Effect

Magic angle effect may be seen in any structure containing collagen fibres and is seen as a result of the dipole interaction between the applied external magnetic field (B_0) and the collagen fibres. This effect results in regions of artefactually increased signal intensity within the structure being imaged on short TE (T1 and proton density) sequences. The phenomenon is maximised when the relative angular orientation of the collagen fibres to the static magnetic field is approximately 55 degrees. Tendons, hyaline cartilage and menisci may all be affected by the magic angle effect which should not be misinterpreted as tendinopathic change or tearing (Fig. 8). Repositioning of the patient in a different orientation to the applied magnetic field or by using sequences with a long echo time (T2-weighted sequences) will eliminate the artefact. When magic angle effect is suspected it is useful to compare the short TE images with the same area on T2 weighted imaging.

2.4.7 Aliasing or Wraparound Artefact

Aliasing or wraparound artefact is seen where an image of tissue from outside the field-of-view (FOV) appears superimposed on images of the area of interest. This may be from a different body part positioned adjacent to the area of interest or the result of parts of the hand or wrist outside the field-of-view being superimposed on the area of interest (Fig. 9). The former is most usually seen when the hand or wrist is positioned by the side of the patient while the latter is particularly common with the small FOV imaging usually employed in hand and wrist imaging. In this case, images of adjacent body parts may be superimposed on the FOV. In both cases the resultant image resembles a double exposure photograph.

All frequency related artefacts are more pronounced at 3T imaging compared with 1.5T imaging (Barth et al. 2007). This includes metal related signal voids and other types of susceptibility artefact related to hemosiderin deposition and at air tissue interfaces as well chemical shift artefact. However, at 3T imaging the increased SNR can be employed to compensate for these artefacts more effectively whilst still maintaining a high degree of spatial resolution.

3 Imaging Findings

3.1 Osseous Structures

T1 weighted images demonstrate osseous anatomy well and are particularly useful for the detection of fracture lines and bone marrow oedema (appearing as a low signal change within the medullary cavity). However, fat suppressed T2 imaging is also sensitive to marrow signal change [seen as increased (fluid) signal] although anatomical definition may be less clearly shown. In cases of non-specific wrist pain, focal bone oedema has been shown to be present in approximately one-third of all cases on MR imaging (Alam et al. 1999); in this study, the causes demonstrated included arthritis, fracture and avascular necrosis.

MR imaging has been proven to be useful post trauma in the context of negative radiographs with particular reference to identifying occult scaphoid fractures (Breitenseher et al. 1997; Hunter et al. 1997). Early confirmation of the diagnosis is possible

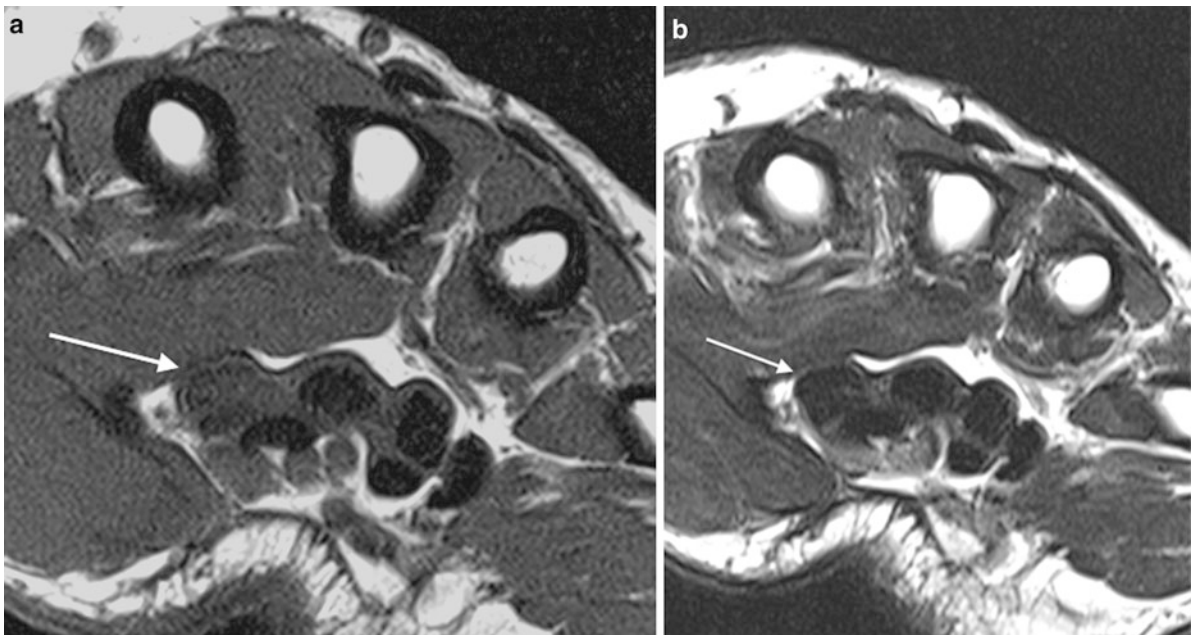


Fig. 8 **a** T1 axial image of the hand distal to the carpal tunnel. There is low signal change seen within the Flexor Pollicis Longus tendon due to magic angle phenomenon (*arrow*). **b** axial

image of the same patient but with altered parameters—this sequence has a long TE value and the magic angle phenomenon is abolished (*arrow*)



Fig. 9 Wraparound artefact—Superimposed ghosting of the splinting flexor tendons is seen at the periphery of the image as a result of wraparound artefact. In addition, there is a ghost image of the thumb to the *left* of the image

with MR imaging as opposed to the previously accepted method of repeating plain radiographs 7–10 days following the initial presentation. MR imaging is also useful for demonstrating the early

stages of avascular necrosis when plain film images appear normal. This is most commonly seen following fracture to the scaphoid in association with non-union. An indicator of developing non-union is sclerosis around the fracture site without evidence of bridging bone. In the advanced stages of the condition findings also include articular surface collapse and fragmentation of the involved bone. Gadolinium sequences are used to assess for the presence of vascularity within the scaphoid where there is concern for avascular necrosis—in this case T1 weighted images show uniform low signal within a necrotic segment and there is no enhancement in a non-viable segment following administration of IV gadolinium.

3.2 Tendons

The extensor tendons situated on the volar aspect of the wrist are divided into six numbered compartments by vertical septae and the extensor retinaculum (Table 1). On the volar aspect of the wrist the eight digital flexor tendons are divided into superficial and deep groups which—along with the flexor pollicis longus tendon which inserts into the distal phalanx of the thumb, pass through the carpal tunnel. The digital flexors share a

Table 1 Extensor tendon compartments

I	Abductor pollicis longus, Extensor pollicis brevis
II	Extensor carpi radialis longus, Extensor carpi radialis brevis
III	Extensor pollicis longus
IV	Extensor digitorum longus
V	Extensor digiti minimi
VI	Extensor carpi ulnaris

common flexor tendon sheath apart from the flexor pollicis longus which has its own sheath. At the level of the carpal tunnel the flexor digitorum superficialis (FDS) tendons lie superficial to the flexor digitorum profundus (FDP) tendons. Each superficial tendon then splits at the level of the proximal phalanx passing either side of the profundus tendon to insert into the middle phalanx. The flexor digitorum profundus continues to insert onto the distal phalanx.

The flexor and extensor tendons of the hand and wrist are best evaluated in an axial plane; normal tendons should appear as homogeneously low signal structures regardless of the imaging sequence used (Fig. 10). Both proton density and T2 weighted sequences in the axial plane are usually sufficient to assess the intrinsic signal characteristics of the tendons and assess for any surrounding fluid. The tendons are susceptible to magic angle effect and the T2 sequence is helpful to rule this out where high signal is seen in tendons on the shorter TE sequence (Fig. 8). A small amount of fluid may be seen within the tendon sheath in normal asymptomatic patients and when seen warrants careful correlation with clinical findings before it is reported as abnormal. Tendinopathy is characterised by high signal change within the tendon. The tendon is frequently also thickened. Tenosynovitis is characterised by circumferential high signal fluid within the tendon sheath (Fig. 11). The tendons which are most frequently affected by tendinosis are those of the first and sixth extensor compartments, namely the abductor pollicis longus and the extensor pollicis brevis (involved in De Quervain's tenosynovitis) and the extensor carpi ulnaris respectively. The latter is particularly frequently affected in rheumatoid arthritis. De Quervain's tenosynovitis is typically associated with thickening of the tendons themselves. In the acute phase fluid may be seen in the tendon

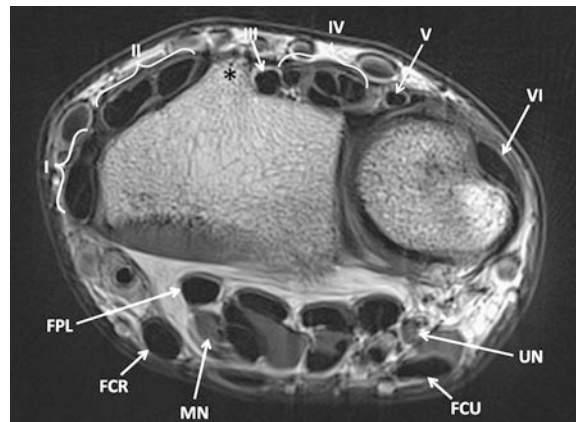


Fig. 10 Axial normal wrist—Axial PD image of the wrist. The tendons appear as homogeneously low signal oval structures. The six extensor compartments are labelled on the volar aspect of the wrist. Lister's tubercle (*asterix*) is a useful landmark on the distal radius which separates compartments II and III

sheath but in the chronic situation thickening of the soft tissue around the compartment (the extensor retinaculum) will be seen. Tenosynovitis of the digital flexors is commonly related to chronic injury, repetitive microtrauma and inflammatory arthropathy. Flexor tendon tenosynovitis is a common cause of carpal tunnel syndrome due to the close anatomical proximity of these tendons to the median nerve.

Coronal sequences of the flexor and extensor tendons are rarely useful owing to partial volume effects which occur in this plane. Sagittal sequences are of most value when assessing abnormalities of the finger flexor and extensor tendons.

3.3 Triangular Fibrocartilage Complex

The TFCC is a fibrocartilage ligament complex which overlies the distal ulna and is not only an important stabiliser of the distal radioulnar joint but also acts as a soft tissue cushion between the distal ulna and the carpus. This complex comprises five components: the triangular fibrocartilage, dorsal and volar radioulnar ligaments, ulnolunate and ulnotriquetral ligaments, the meniscal homologue and the extensor carpi ulnaris (ECU) tendon sheath (Fig. 12). The thickness of the TFCC varies from 2 to 5 mm and depends upon the configuration of the joint space—negative ulnar variance will lead to a thicker TFCC and conversely positive variance will lead to

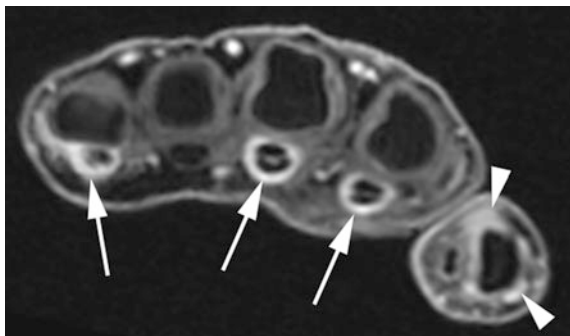


Fig. 11 Tenosynovitis—Axial T1W imaging post gadolinium administration in a patient with rheumatoid arthritis shows circumferential enhancing soft tissue within the flexor tendon sheath of the little, middle and index fingers separating the deep and superficial flexor tendons and representing tenosynovitis. In addition, there is marked enhancing synovitis seen thumb MCP joint (*arrowheads*)

a thinner structure. Its radial attachment is to the articular cartilage of the sigmoid notch of the radius. There are two distinct ulnar attachments, the first to the ulnar fovea at the styloid base and the second to the styloid process of the ulnar. Separating these two areas of insertion is an area of connective tissue known as the ligamentum subcruentum (Nakamura et al. 1996). The blood supply to the TFCC comes from three sources: the ulnar artery and both the palmar and dorsal branches of the anterior interosseous artery. These vessels penetrate the peripheral aspect of the TFCC however the central and radial portions are avascular. Consequently, the peripheral portion has the potential to heal following repair whereas the central and radial portions do not.

Assessment of the integrity, thickness and signal characteristics of the TFCC is optimal in the coronal plane where the articular disc, the meniscal homologue, triangular ligament and ulnotriquetral ligament are all well visualised. The dual attachment of the TFCC to the ulnar is also best appreciated in this plane, where insertion into both the ulnar styloid tip and the fovea are seen. It is important not to mistake this bifid attachment for a tear. In addition the axial plane will better demonstrate the volar and dorsal radioulnar ligaments. The sagittal plane is also useful in visualising the ulnar foveal attachment (Amrami and Felmlee 2008).

The articular disc of the TFCC is seen on high resolution MR imaging as a low to intermediate signal



Fig. 12 Normal TFCC anatomy—coronal T2 FS image shows a normal TFCC. The bifid ulnar attachment (*white arrows*) may be seen here as well as the radial attachment. At the radial attachment hyaline cartilage is seen interposed between the TFCC and the bone (*black arrow*)—this appearance should not be misinterpreted as a TFCC tear. In this case, there is a tear of the scapholunate ligament with consequent widening of the scapho-lunate distance (*arrowheads*)

intensity band with slightly higher signal characteristics seen within the ulnar attachment on proton density and T2 star weighted images. Perforations or tears of the TFCC structure are seen as discrete areas of high signal intensity coursing through the substance of the articular disc. Degenerative change will manifest as an area of high signal intensity within the articular disc but without extension to the articular surface (Fig. 13). The radial attachment of the triangular fibrocartilage is onto hyaline cartilage and on conventional MRI this will appear as relatively high signal between the cortical bone and fibrocartilage, an important pitfall when diagnosing radial attachment tears.

Several studies have confirmed the role of MR imaging in diagnosing TFCC pathology. However, the performance of standard MRI in the diagnostic work-up of TFCC tears is highly dependent upon the location of the lesion. Studies have demonstrated that for central and radial sided TFCC tears sensitivity and specificity is in the region of 90 % when compared with arthroscopy. However, for peripheral attachment tears sensitivity and specificity are much lower. The relatively low yield of MRI for peripheral tears is primarily attributed to the false positive results induced by the high signal of the ligamentum



Fig. 13 Degenerative TFCC—PD FS coronal image shows. This case shows a patient with ulnar lunate abutment syndrome. There is bone oedema seen with the proximal aspect of the lunate (*white arrow*) and diffuse intrinsic high signal is seen within the radial central portion of the TFCC representing degenerative change within the fibrocartilage (*arrowhead*). This high signal does not extend to the articular surface and should not be misinterpreted as a tear

subcrucium on T2-weighted sequences along with the abnormal signal that may stem from degenerative changes of fibrocartilage. Tears affecting the central portion of the articular disc are generally felt to have a degenerative aetiology and are often asymptomatic. Asymptomatic perforations are a frequent finding in the triangular fibrocartilage even in young patients, one study reporting 51 % of asymptomatic wrists showing perforations (Brown et al. 1994). Peripheral tears tend to be traumatic in nature, often symptomatic and necessitate surgical intervention.

In view of the limitations of conventional MRI, MR arthrography is frequently advocated as the investigation of choice for the assessment of TFCC injury (Fig. 14). Proponents of conventional MRI suggest the use of 3D volumetric acquired gradient recalled sequences for evaluating the TFCC and have shown sensitivity of 100 %, specificity of 90 % and an accuracy of 97 % when using arthroscopy as the gold standard (Potter et al. 1997).



Fig. 14 Full thickness TFC tear. Coronal T1 fat suppressed image from MR arthrogram. Iodinated contrast injected into the radiocarpal joint at the time of the arthrogram was seen on fluoroscopy to pass into the distal radioulnar joint so only a single injection was undertaken. MRI shows the full thickness perforation through the triangular fibrocartilage (*arrow*) representing a full thickness tear and the passage through which contrast has passed between the two compartments. This is traumatic Palmer type 1A tear

3.4 Ligaments

3.4.1 The Intrinsic Ligaments

The intrinsic ligaments of the wrist are crucial to the intrinsic stability of the joint. These ligaments pass between the carpal bones without attachment to the radius or ulnar. The scapholunate ligament and the lunotriquetral ligament are clinically the most important and imaging is often integral in determining the extent of pathology related to these structures. The two ligaments are responsible for the stabilisation of the bones of the proximal carpal row and their disruption is an important component of dissociative carpal instability. Both the ligaments have three distinct components, namely the dorsal, volar and proximal. The scapholunate ligament is C shaped whereas the lunotriquetral ligament appears V shaped. The proximal portions of both these ligaments are thin fibrocartilaginous membranes with no stabilizing role. However, the fibrous volar and dorsal components act as true ligaments preventing independent flexion and extension of the proximal carpal bones so the entire unit acts as an intercalated segment (Fig. 15).

Fig. 15 Normal Intrinsic ligaments—T2 FS coronal image of the wrist shows both the scapholunate (*white arrow*) and lunate-triquetral (*black arrow*) ligaments



Fig. 16 Normal Extrinsic Ligaments. Coronal image from an arthrographic study shows part of the radioscapholunate and radioscaphocapitate extrinsic ligaments on the volar aspect of the wrist

Although scapholunate ligament injuries are usually assessed on conventional radiographic imaging in the first instance, MR imaging, and particularly MR arthrography plays an increasingly important role in diagnosing injuries of the intrinsic ligaments.

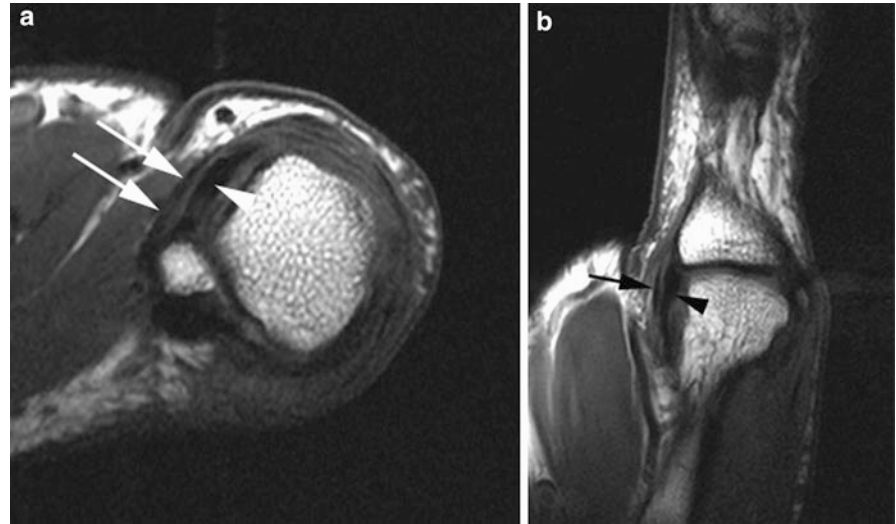
Conventional radiographs will only show abnormality where there is either an increased scapholunate gap or alteration in alignment between bones of the proximal carpal row.

Both CT and MR arthrography are more sensitive than standard MR imaging in the detection of scapholunate tears, particularly for more subtle injuries (Cerezal et al. 2005). The use of MR arthrography may allow more accurate delineation of the exact location of a tear allowing differentiation between lesions which are degenerate in nature and predominantly affecting the membranous portion of the ligament from acute injuries which involve either or both of the dorsal or volar components.

3.4.2 The Extrinsic Ligaments

The extrinsic ligaments are classified as either volar or dorsal; the volar ligaments are considered to be important stabilisers of the wrist whereas the dorsal ligaments are thought to be less crucial for stability (Theumann et al. 2003). The volar ligaments on the radial aspect of the wrist comprise the radioscaphocapitate, the radiolunatotriquetral and the radioscapholunate ligaments. On the ulnar aspect of the wrist there are two main volar ligaments which also form part of the triangulofibrocartilage (TFCC) complex, namely the ulnolunate and the ulnotriquetral ligaments. On the dorsal aspect of the wrist the extrinsic ligaments form a V shape centred over the dorsal aspect of the triquetrum. These ligaments are areas of focal thickening within the joint capsule and are often difficult to visualise with both MR and MR arthrography (Fig. 16).

Fig. 17 Ulnar collateral ligament of the thumb—**a** and **b** shows axial and coronal imaging of a normal UCL in the thumb. Both the ulnar collateral ligament (*white arrow*) itself and the overlying adductor aponeurosis are shown (*arrowheads*)



An avulsion injury of these extrinsic ligaments from their triquetral attachment is the cause of the triquetral fracture best appreciated on a lateral wrist radiograph.

3.4.3 The Ulnar Collateral Ligament of the Thumb

The Ulnar Collateral Ligament of the Thumb is also generally assessed with MRI, although ultrasound can also usefully image this frequently injured ligament. Overlying the normal ligament a thin adductor aponeurosis is identified (Fig. 17a, b). The ulnar collateral ligament stabilises the thumb metacarpophalangeal joint against radial deviation and its injury is frequently termed gamekeepers skiers thumb. When torn the adductor aponeurosis may interpose itself between the torn ends of the ligament, known as a Stener lesion, preventing healing without intervention. Failure of the torn ligament to heal results in instability and ultimately early osteoarthritis at the joint.

3.5 Hyaline Cartilage

Despite their marked clinical impact, cartilage lesions of the radiocarpal and intercarpal joints are frequently underestimated with MRI and MR arthrography possibly due to their small and subtle nature. High spatial resolution and tissue contrast is needed to detect these subtle changes. At 3T, the SNR is

sufficient but interpretation is complicated by the increased chemical shift artefact at the articular cartilage–bone interface (Fig. 6). Arthroscopy has been shown to be superior to both these imaging methods in the assessment of cartilage damage (Mutimer et al. 2008).

Much of the work regarding cartilage assessment has focussed on imaging of the knee. Various different protocols have been evaluated in this context including fat suppressed 3D spoiled GE, fast SE and direct arthrography (Gold et al. 2003). Three-dimensional GE are useful in cartilage evaluation as a high signal-to-noise ratio is afforded and allows thin slices to be produced, in addition the image may be reconstructed in different planes. These properties have not been shown to easily transfer to imaging of the cartilage within the wrist (Haims et al. 2004). This is thought in part to be due to the thickness of the cartilage at the wrist as well as the other potential difficulties with wrist imaging such as field inhomogeneity and patient movement. Therefore, an optimum method for cartilage evaluation at the wrist remains elusive at present.

4 MR Arthrography

MR arthrography is primarily indicated for the following suspected pathologies:

- Triangular fibrocartilage complex tears
- Scapho-lunate or lunate-triquetral ligament tears

- Suspected cartilage damage/intra-articular body

Communication, and therefore passage of contrast, between the radiocarpal joint and other compartments has been described in asymptomatic patients and findings therefore need to be carefully correlated with the clinical situation. A communication between the radiocarpal and midcarpal compartments has been described in 13–47 % of the population and between the radiocarpal and distal radioulnar compartments in 7–35 % of the population (Manaster 1991; Wilson et al. 1991; Cantor et al. 1994).

4.1 Protocols

As is the case with standard MR, imaging protocols for arthrographic imaging will vary between institutions. However, T1 weighted imaging will form the basis of the study showing the gadolinium arthrographic contrast as high signal. While T1 fat suppressed imaging has advantages in increasing contrast and also clarifying high signal due to contrast as opposed to fat, it is important to include at least one T1 weighted sequence without fat suppression for bony detail. It is also helpful to include a water sensitive (T2 fat suppressed) sequence to look for soft tissue pathology outside the joint itself and also for demonstrating oedematous change in bone marrow. The authors employ this sequence in the coronal plane.

4.2 Injection of Contrast

Since the first description of wrist arthrography by Kessler and Silberman (1961), many different methods, protocols and injection techniques have been described. Intra-articular injection of contrast material for the purposes of performing an MR arthrogram is usually performed under fluoroscopic guidance, although ultrasound guided injection may be used. The advantage of using fluoroscopic guidance is that a dynamic assessment for carpal instability can be made at the same time, and also fluoroscopic screening during contrast injection may demonstrate passage of contrast into adjacent compartments through ligament or fibrocartilage tears.

Single, double and triple compartment injection techniques have been described (Cerezal et al. 2005; Malfair 2008). The single compartment technique involves injection into the radiocarpal joint usually via



Fig. 18 Undersurface Flap tear of the TFCC—In this case the DRUJ was injected with contrast as well as the radiocarpal joint. This coronal image shows a partial thickness undersurface tear of the TFCC (*white arrow*) outlined by contrast injected into the DRUJ. This tear may not have been appreciated with a single radiocarpal joint injection

a dorsal approach. However, a lateral approach has also been described (Medverd et al. 2011). Because of the dorsal lip which overlies the radiocarpal joint on an AP image slight proximal angulation of the image intensifier will allow improved visualisation of the joint.

When investigating possible TFCC injury a double compartment technique is useful with a second injection into the DRUJ to outline the proximal (undersurface) of the triangular fibrocartilage (Fig. 18). This technique is useful for demonstrating partial ulnar attachment tears which are frequently non-communicating and may only be seen at the proximal attachment which may not be visible when contrast is only injected into the radiocarpal joint (Ruegger et al. 2007; Burns et al. 2011).

In the normal situation intact scapholunate and lunatetriquetral ligaments should prevent flow of contrast passage of contrast into the midcarpal joint from the radiocarpal joint and such passage will indicate a perforation or tear (which may be asymptomatic) through one of these ligaments. Conventional arthrographic studies have indicated that flow

may be one way through tears in these ligaments and there may be an advantage to injecting the midcarpal joint (Levinsohn et al. 1987, 1991; Wilson et al. 1991). However, with the direct visualisation of the intrinsic ligaments afforded by MRI it is not clear that a midcarpal joint injection offers any advantages when arthrography is combined with MRI.

4.3 Artefacts

Besides artefacts seen using conventional MRI and described in 2.4 there are additional artefacts which need to be considered in arthrography. These primarily relate to the injectate and injection technique. Injected air bubbles may mimic intra-articular bodies and care should be taken to eliminate any air bubbles from the injected system wherever possible. Injectate or local anaesthetic which has been inadvertently injected into muscle or surrounding soft tissue may be confused for oedematous change or contusion.

4.4 Indirect Arthrography

Indirect arthrography is also advocated to improve the diagnostic accuracy of standard MR sequences and is considered less invasive than direct arthrography. In this technique, intravenous contrast diffuses into the joint in a concentration high enough that an arthrographic effect may be achieved on T1 weighted images, although clearly the joint is not distended as with direct arthrography. Studies have reported the increased sensitivity in evaluation of the scapholunate ligament using indirect arthrography when compared with unenhanced MRI of the wrist but this has not been shown to be the case in evaluation of the lunatetriquetral ligament (Haims et al. 2003).

4.5 Alternative Modalities

Other imaging modalities should also of course be considered and recent studies have shown Multidetector CT (MDCT) arthrography to be more accurate than both 1.5T MR imaging and MR arthrography for the detection of partial tears of the scapholunate and lunatotriquetral ligaments (Schmid et al. 2005; Moser et al. 2007). CT arthrography offers advantages in terms of spatial resolution despite the absence of soft tissue contrast. An extremely small pilot study has shown

similar performance for direct MR arthrography and CT arthrography for the depiction of the triangular fibrocartilage although no attempt was made to evaluate the accuracy of these techniques for diagnosing tears (Omlor et al. 2009).

5 7T Imaging

7T imaging is a technique which is potentially particularly useful in the hand and wrist owing to its superior signal to noise ratio which allows higher spatial resolution; a quality which would allow even more detailed imaging of the fine anatomical structures of the hand and wrist, particularly the TFCC, intrinsic ligaments and articular cartilage. At present, this technique is limited to research purposes and presents many technical difficulties. These include the need for specialised RF coils which are currently not commercially widely available and the increasing chemical shift artefact encountered with increasing field strength. A potential future direction will be the opportunities 7T imaging offers for enhancing biological imaging techniques such as spectroscopy, sodium imaging and delayed gadolinium-enhanced MRI of cartilage (dGEMRIC) which will benefit significantly from the signal-to-noise gains at increased field strengths with particular advantages when applied to the smaller structures of the hand and wrist.

References

- Alam F, Schweitzer ME, Li XX, Malat J, Hussain SM (1999) Frequency and spectrum of abnormalities in the bone marrow of the wrist: MR imaging findings. *Skeletal Radiol* 28(6):312–317
- Amrami KK, Felmlee JP (2008) 3-Tesla imaging of the wrist and hand: techniques and applications. *Semin musculoskelet radiol* 12(3):223–237
- Barth MM, Smith MP, Pedrosa I, Lenkinski RE, Rofsky NM (2007) Body MR imaging at 3.0 T: understanding the opportunities and challenges. *Radiographics* 27(5): 1445–1462 discussion 1462–1444
- Blackband SJ, Chakrabarti I, Gibbs P, Buckley DL, Horsman A (1994) Fingers: three-dimensional MR imaging and angiography with a local gradient coil. *Radiology* 190(3): 895–899
- Breitenseher MJ, Metz VM, Gilula LA, Gaebler C, Kukla C, Fleischmann D et al (1997) Radiographically occult scaphoid fractures: value of MR imaging in detection. *Radiology* 203(1):245–250

- Brown JA, Janzen DL, Adler BD, Stothers K, Favero KJ, Gropper PT et al (1994) Arthrography of the contralateral, asymptomatic wrist in patients with unilateral wrist pain. *Can Assoc Radiol J* 45(4):292–296
- Burns JE, Tanaka T, Ueno T, Nakamura T, Yoshioka H (2011) Pitfalls that may mimic injuries of the triangular fibrocartilage and proximal intrinsic wrist ligaments at MR imaging. *Radiographics : a review publication of the Radiological Society of North America* 31(1):63–78
- Cantor RM, Stern PJ, Wyrick JD, Michaels SE (1994) The relevance of ligament tears or perforations in the diagnosis of wrist pain: an arthrographic study. *J Hand Surg* 19(6):945–953
- Cerezal L, Abascal F, Garcia-Valtuille R, Del Pinal F (2005) Wrist MR arthrography: how, why, when. *Radiologic clin N Am* 43(4):709–731
- Farooki S, Ashman CJ, Yu JS, Abduljalil A, Chakeres D (2002) In vivo high-resolution MR imaging of the carpal tunnel at 8.0 tesla. *Skeletal Radiol* 31(8):445–450
- Gold GE, McCauley TR, Gray ML, Disler DG (2003) What's new in cartilage? *Radiographics : a review publication of the Radiological Society of North America* 23(5):1227–1242
- Haims AH, Moore AE, Schweitzer ME, Morrison WB, Deely D, Culp RW et al (2004) MRI in the diagnosis of cartilage injury in the wrist. *AJR Am J Roentgenol* 182(5):1267–1270
- Haims AH, Schweitzer ME, Morrison WB, Deely D, Lange RC, Osterman AL et al (2003) Internal derangement of the wrist: indirect MR arthrography versus unenhanced MR imaging. *Radiology* 227(3):701–707
- Hauger O, Chung CB, Lektrakul N, Botte MJ, Trudell D, Boutin RD et al (2000) Pulley system in the fingers: normal anatomy and simulated lesions in cadavers at MR imaging, CT, and US with and without contrast material distention of the tendon sheath. *Radiology* 217(1):201–212
- Hunter JC, Escobedo EM, Wilson AJ, Hanel DP, Zink-Brody GC, Mann FA (1997) MR imaging of clinically suspected scaphoid fractures. *AJR Am J Roentgenol* 168(5):1287–1293
- Kessler I, Silberman Z (1961) An experimental study of the radiocarpal joint by arthrography. *Surg Gynecol Obstet* 112:33–40
- Kocharian A, Adkins MC, Amrami KK, McGee KP, Rouleau PA, Wenger DE et al (2002) Wrist: improved MR imaging with optimized transmit-receive coil design. *Radiology* 223(3):870–876
- Levinsohn EM, Palmer AK, Coren AB, Zinberg E (1987) Wrist arthrography: the value of the three compartment injection technique. *Skeletal Radiol* 16(7):539–544
- Levinsohn EM, Rosen ID, Palmer AK (1991) Wrist arthrography: value of the three-compartment injection method. *Radiology* 179(1):231–239
- Magee T (2009) Comparison of 3-T MRI and arthroscopy of intrinsic wrist ligament and TFCC tears. *AJR Am J Roentgenol* 192(1):80–85
- Malfair D (2008) Therapeutic and diagnostic joint injections. *Radiologic Clin N Am* 46(3):439–453
- Manaster BJ (1991) The clinical efficacy of triple-injection wrist arthrography. *Radiology* 178(1):267–270
- Medverd JR, Pugsley JM, Harley JD, Bhargava P (2011) Lateral approach for radiocarpal wrist arthrography. *AJR Am J Roentgenol* 196(1):W58–W60
- Moser T, Dosch JC, Moussaoui A, Dietemann JL (2007) Wrist ligament tears: evaluation of MRI and combined MDCCT and MR arthrography. *AJR Am J Roentgenol* 188(5):1278–1286
- Mutimer J, Green J, Field J (2008) Comparison of MRI and wrist arthroscopy for assessment of wrist cartilage. *J Hand Surg* 33(3):380–382
- Nakamura T, Yabe Y, Horiuchi Y (1996) Functional anatomy of the triangular fibrocartilage complex. *J Hand Surg* 21(5):581–586
- Omlor G, Jung M, Grieser T, Ludwig K (2009) Depiction of the triangular fibro-cartilage in patients with ulnar-sided wrist pain: comparison of direct multi-slice CT arthrography and direct MR arthrography. *Eur Radiol* 19(1):147–151
- Potter HG, Asnis-Ernberg L, Weiland AJ, Hotchkiss RN, Peterson MG, McCormack RR Jr (1997) The utility of high-resolution magnetic resonance imaging in the evaluation of the triangular fibrocartilage complex of the wrist. *J Bone Joint Surg* 79(11):1675–1684
- Roemer PB, Edelstein WA, Hayes CE, Souza SP, Mueller OM (1990) The NMR phased array. *MRM: official journal of the society of magnetic resonance in medicine/society of magnetic resonance in medicine* 16(2):192–225
- Ruegger C, Schmid MR, Pfirrmann CW, Nagy L, Gilula LA, Zanetti M (2007) Peripheral tear of the triangular fibrocartilage: depiction with MR arthrography of the distal radioulnar joint. *AJR Am J Roentgenol* 188(1):187–192
- Saupe N, Prussmann KP, Luechinger R, Bosiger P, Marincek B, Weishaupt D (2005) MR imaging of the wrist: comparison between 1.5- and 3-T MR imaging—preliminary experience. *Radiology* 234(1):256–264
- Schmid MR, Schertler T, Pfirrmann CW, Saupe N, Manestar M, Wildermuth S et al (2005) Interosseous ligament tears of the wrist: comparison of multi-detector row CT arthrography and MR imaging. *Radiology* 237(3):1008–1013
- Stevens KJ, Wallace CG, Chen W, Rosenberg JK, Gold GE (2011) Imaging of the wrist at 1.5 Tesla using isotropic three-dimensional fast spin echo cube. *JMRI* 33(4):908–915
- Tan AL, Grainger AJ, Tanner SF, Shelley DM, Pease C, Emery P et al (2005) High-resolution magnetic resonance imaging for the assessment of hand osteoarthritis. *Arthritis Rheum* 52(8):2355–2365
- Theumann NH, Pfirrmann CW, Antonio GE, Chung CB, Gilula LA, Trudell DJ et al (2003) Extrinsic carpal ligaments: normal MR arthrographic appearance in cadavers. *Radiology* 226(1):171–179
- Wilson AJ, Gilula LA, Mann FA (1991) Unidirectional joint communications in wrist arthrography: an evaluation of 250 cases. *AJR Am J Roentgenol* 157(1):105–109